Chapter 2

Non-linear models for High Power Amplifiers

In this chapter we start by developing the analytical formulation of a general structure for the nonlinear distortion. This formulation, based on the Volterra series expansion, is provided in order to demonstrate the validity of some classical approximations concerning the use of higher order nonlinear models for HPA characterization. Then, one of the most validated HPA models is described in some detail for its later use in our simulations. The theoretical relations between its direct and inverse characteristics are included since they constitute an important qualitative reference for the pre-distortion algorithms. Finally, some foresight about certain limiting aspects on the invertibility of complex nonlinearities is given and some graphical examples are briefly discussed.

The study of nonlinearities and their effects in communications systems can be carried out through the analytical treatment of models that are conceived to approach the fundamental physical nature of the devices and channels. Such treatment, often based on solving non-trivial sets of differential equations (normally untractable by algebraic means), lead us to seek the aid of numeric methods and further simplifications to face the almost unbeatable mathematical challenges therein involved. Hence, higher-level transference models, normally referred to as 'behavioural' models, are required for producing testable characterizations of nonlinearities by providing good accuracy at a reasonable complexity for analysis as well as simulation purposes. For the representation of nonlinear HPAs, input-output block models are mainly of two types: instantaneous or memoryless models and models with memory. All of these models use either a limited or unlimited number of parameters that are adjustable by means of fitting procedures to represent the input-output functional relationship of a given real system. In the case of unlimited coefficients (as in the case of the series expansion), the number of independent components is normally restricted according to specific criteria, which is related in communications to measures of significance of each component in the general nonlinear behaviour. In turn, nonlinear models based on a limited set of parameters offer

simpler configurations and are accurate enough to represent or identify many nonlinear systems. However, in some cases even memoryless models with few-parameters present some specific inaccuracies and non-physical behaviours (e.g. the limitations of the Cann's model shown by Loika in [42]). These characterizations should be therefore carefully applied under the restrictions found for each specific case. Thus, although some models have become classical through their widespread application, they always deserve to be reviewed in some detail or, at least, previously discussed before their application in the specific scenario for which they have been selected.

2.1 Volterra Series Model for Memoryless Non-linearities

This section addresses the general formulation of the non-linear AM/AM–AM/PM distortion starting from a Volterra Series Model which is used, under some restrictions, to describe the general structure of the nonlinear effects considered in the thesis.

The Volterra series have been widely used in non-linear systems modeling and analysis. They provide an appealing and quite general functional representation of the relation between the output and the input of a nonlinear time-invariant system (TI-NLS) with or without memory [43]. The Volterra Series Model (VSM) can be seen as a generalization of the Taylor Series expressed in the form

$$\begin{aligned} y(t) \;=\; & h_0 + \int_{-\infty}^{\infty} h_1(\tau_1)x(t-\tau_1)d\tau_1 + \int_{-\infty}^{\infty}\int_{-\infty}^{\infty} h_2(\tau_1,\tau_2)x(t-\tau_1)x(t-\tau_2)d\tau_1 d\tau_2 \\ & + \int_{-\infty}^{\infty}\int_{-\infty}^{\infty}\int_{-\infty}^{\infty} h_3(\tau_1,\tau_2,\tau_3)x(t-\tau_1)x(t-\tau_2)x(t-\tau_3)d\tau_1 d\tau_2 d\tau_3 + \cdots \\ & + \int_{-\infty}^{\infty}\cdots\int_{-\infty}^{\infty} h_n(\tau_1,\tau_2,\cdots,\tau_n)x(t-\tau_1)x(t-\tau_2)\cdots x(t-\tau_n)d\tau_1 d\tau_2\cdots d\tau_n + \cdots \end{aligned} \tag{2.1}$$

where, for $n = 1, 2, \ldots$, the system is defined as causal with

$$h_n(\tau_1, \ldots, \tau_n) = 0, \forall\ \tau_i < 0,\ i = 1, 2, \ldots, n. \tag{2.2}$$

The functions $\{h_o, h_1(\tau), h_2(\tau_1, \tau_2), \ldots\}$ are called the *Volterra kernels* of the system. The zero-order term h_0 represents the system response to a continuous (dc) input. The first-order kernel h_1 is the linear impulse response of the system while the higher-order kernels ($n \geq 2$) can also be considered as multi-dimensional impulse responses that characterize the higher order non-linearities of the system [44]. The VSM can be particularized to consider the memoryless case of a system if the kernels are defined

as delta functions $\delta_m(\tau_1, \ldots, \tau_m)$ centered with respect to the m-dimensional origin. In such a case, the VSM becomes a polynomial expansion like the Taylor series model [45].

The general VS model is herein particularized for the case of a bandpass system. First, let the base-band input signal model be

$$b_x(t) = u_x(t)e^{j\alpha_x(t)} \tag{2.3}$$

where $u_x(t) = |b_x(t)|$. Thence, the bandpass input signal model for the analysis will be defined as follows:

$$x(t) = \mathrm{Re}\{b_x(t)e^{j2\pi f_c t}\} = \frac{1}{2}b_x(t)e^{j2\pi f_c t} + \frac{1}{2}b_x^*(t)e^{-j2\pi f_c t}. \tag{2.4}$$

Replacing $\omega_c = 2\pi f_c$ for brevity and using eqs. (2.1) and (2.4), we obtain

$$\begin{aligned} y(t) \;=\; & h_0 + \int_{-\infty}^{\infty} h_1(\tau_1)\mathrm{Re}\{b_x(t-\tau_1)e^{j\omega_c(t-\tau_1)}\}d\tau_1 \\ & + \int_{-\infty}^{\infty}\int_{-\infty}^{\infty} h_2(\tau_1,\tau_2)\mathrm{Re}\{b_x(t-\tau_1)e^{j\omega_c(t-\tau_1)}\}\mathrm{Re}\{b_x(t-\tau_2)e^{j\omega_c(t-\tau_2)}\}d\tau_1 d\tau_2 \\ & \cdots + \int_{-\infty}^{\infty}\cdots\int_{-\infty}^{\infty} h_n(\tau_1,\tau_2,\cdots,\tau_n)\prod_{i=1}^{n}\mathrm{Re}\{b_x(t-\tau_i)e^{j\omega_c(t-\tau_i)}\}d\tau_i + \cdots \end{aligned} \tag{2.5}$$

The following narrow-band approximations will apply for this model:

$$B_x \ll f_c \;\;;\;\; \mathcal{T}_i \ll \frac{1}{B_x}\;,\; i = 1, 2, \ldots, n \tag{2.6}$$

where the carrier frequency f_c is defined much larger than the bandwidth of the input base-band signal B_x, while the time span given by the inverse of this last is larger than the duration $\mathcal{T}_i$ of any i-th component of the kernels $h_n(\tau_1, \ldots, \tau_n)$ defined for the multi-dimensional convolution in (2.5). According to this, the kernels are characterized as approximated delta functions. Then, for $i = \{1, 2, \ldots, n\}$ these conditions are declared valid and allow us to consider that for the base-band information signal we can assume

$$b_x(t-\tau_i) \approx b_x(t)\;;\; \forall\, |\tau_i| \leq \mathcal{T}_i \tag{2.7}$$

which leads us to a memoryless approximation with regard to the base-band equivalent of the non-linear system. However, the equivalent approximation in the passband phase component,

$$e^{j\omega_c(t-\tau_i)} \approx e^{j\omega_c(t)}, \tag{2.8}$$

is not valid since $\omega_c\tau_i$ will result in a significant quantity and cannot be neglected. Then, from (2.5) and using the narrowband approximations, the VSM for the range $i = \{1, \ldots, n\}$ can be converted to

$$y(t) = h_0 + \sum_{m=1}^{n} \underbrace{\int_{-\infty}^{\infty} \cdots \int_{-\infty}^{\infty}}_{m-\text{times}} h_m(\tau_1, \ldots, \tau_m) \prod_{i=1}^{m} \text{Re}\{b_x(t)e^{j\omega_c(t-\tau_i)}\} d\tau_m. \tag{2.9}$$

Since the real part operator Re{ } is given by

$$\text{Re}\{b_x(t)e^{j\omega_c(t-\tau_i)}\} = \frac{1}{2}\Big[b_x(t)e^{j\omega_c(t-\tau_i)} + b_x^*(t)e^{-j\omega_c(t-\tau_i)}\Big] \tag{2.10}$$

then, from (2.3) and (2.10) we can rewrite the product in (2.9) as follows:

$$\begin{aligned}
\prod_{i=1}^{m} \text{Re}\{b_x(t)e^{j\omega_c(t-\tau_i)}\} &= \prod_{i=1}^{m} \text{Re}\{u_x(t)e^{j[\omega_c(t-\tau_i)+\alpha_x(t)]}\} \\
&= \left(\frac{u_x(t)}{2}\right)^m \prod_{i=1}^{m} \left(e^{j[\omega_c(t-\tau_i)+\alpha_x(t)]} + e^{-j[\omega_c(t-\tau_i)+\alpha_x(t)]}\right) \quad (2.11) \\
&= \left(\frac{u_x(t)}{2}\right)^m \sum_{\ell=0}^{m} \sum_{\ell'=1}^{C_{(m,\ell)}} e^{j\left[\left(m-2\ell\right)\left(\omega_c t+\alpha_x(t)\right)+\omega_c\Theta(\ell,\ell')\right]}. \quad (2.12)
\end{aligned}$$

In these expressions, the product in (2.11) has been equivalently expressed as a sub-grouped sum in (2.12). The parameter $\Theta(\ell, \ell')$ stands for the summation $\sum_{i=1}^{m}(\pm)\tau_i$, where the values τ_i assume positive or negative sign according to the different combinations of "ℓ" conjugated elements and "$m - \ell$" non-conjugated elements defined for each term indexed by "ℓ'". This last expression is obtained by analyzing the product of m complex binomials of the form

$$\prod_{i=1}^{m}(a_i + a_i^*) \tag{2.13}$$

where $a_i = a_I + ja_Q$, $a_i \in \mathbb{C}\ \forall\ i = 1, \ldots, m$.

The expansion of (2.13) results in a summation of 2^m terms. Each term thereof corresponds to a product of the m different complex values a_i ($i = \{1, \ldots, m\}$) where, in turn, each element of such product can assume one of two states: a_i or a_i^*. For example, we can observe the expansion of (2.13) for $m = 3$:

$$\prod_{i=1}^{3}(a_i+a_i^*) = \underset{0\,0\,0}{a_1a_2a_3} + \underset{0\,0\,1}{a_1a_2a_3^*} + \underset{0\,1\,0}{a_1a_2^*a_3} + \underset{0\,1\,1}{a_1a_2^*a_3^*} + \underset{1\,0\,0}{a_1^*a_2a_3} + \underset{1\,0\,1}{a_1^*a_2a_3^*} + \underset{1\,1\,0}{a_1^*a_2^*a_3} + \underset{1\,1\,1}{a_1^*a_2^*a_3^*} \tag{2.14}$$

where a binary code is assigned to each term to make combinatorial relations more evident. Thence, for any m, the resulting 2^m summation terms will span all the different "binary" combinations of "ℓ" ($\leq m$) conjugated elements a_i^* multiplied by "$(m-\ell)$" non-conjugated elements $a_{i'}$, with $i \neq i'$. Hence, the 2^m terms of the expansion can be grouped into $(m+1)$ sub-groups of $C_{(m,\ell)}$ summation terms each, where $C_{(m,\ell)}$ accounts for the number of terms having ℓ conjugated multiplicative elements in any order, in other words, $C_{(m,\ell)} = \binom{m}{\ell} = \frac{m!}{\ell!(m-\ell)!}$ for $\ell = \{0,\ldots,m\}$. Thus, for the previous example shown in (2.14) we have that: $\{C_{(3,0)}=1, C_{(3,1)}=3, C_{(3,2)}=3, C_{(3,3)}=1\}$.

Thence, substituting (2.12) into (2.9), we obtain

$$y(t) = h_0 + \sum_{m=1}^{n} \underbrace{\int_{-\infty}^{\infty}\cdots\int_{-\infty}^{\infty}}_{m-\text{times}} h_m(\tau_1,\ldots,\tau_m)\left(\frac{u_x(t)}{2}\right)^m \sum_{\ell=0}^{m}\sum_{\ell'=1}^{C_{(m,\ell)}} e^{j\left[\left(m-2\ell\right)\left(\omega_c t+\alpha_x(t)\right)+\omega_c\Theta(\ell,\ell')\right]} d\tau_m^{\Pi} \tag{2.15}$$

where, for the sake of brevity, the product $\prod_{i=1}^{m} d\tau_m$ is referred to as $d\tau_m^{\Pi}$ henceforth. Then, given the different $m+1$ values of $(m-2\ell)$ in the exponent of (2.15), we will be interested in filtering only the significant components from the corresponding harmonic sequence. These spectral components are those centered around $\pm w_c$ and form the so called "first" or "principal zone" output $y_1(t)$ of the non-linear system. This partial signal $y_1(t)$ can be obtained from (2.15) by taking $(m-2\ell) = \pm 1$ or, equivalently, $\ell = \frac{m\mp 1}{2}$. Therefore, we will consider only odd values of m, which is a valid constraint since only odd power nonlinearity terms contribute to the first or principal zone output of a non-linear bandpass system [44]. As in the Taylor series approximation, the even-order terms of a nonlinear model generate spectral components that are at least ω_c away from the center passband frequency. This fact can also be applied to the VSM structure whence the first-zone output of the HPA can be "filtered" out from (2.15) resulting in

$$y_1(t) = \sum_{m=1}^{n} \underbrace{\int_{-\infty}^{\infty}\cdots\int_{-\infty}^{\infty}}_{m-\text{times}} h_m(\tau_1,\ldots,\tau_m)\left(\frac{u_x(t)}{2}\right)^m \underbrace{\sum_{\ell=\frac{m\mp 1}{2}}\sum_{\ell'=1}^{C_{(m,\ell)}} e^{j\left[\left(m-2\ell\right)\left(\omega_c t+\alpha_x(t)\right)+\omega_c\Theta(\ell,\ell')\right]} d\tau_m^{\Pi}}_{\text{filtered terms}} \tag{2.16}$$

where $m = 1,3,5,7,\ldots,n$ (odd). Since the index ℓ takes only two values, henceforth we will declare $C_{(m,\ell)}$ as dependent only on m. Moreover, the resulting number of additive

terms $C_{(m)}$ within the sub-groups, with $\ell = \frac{m\mp1}{2}$ conjugated multiplicative elements, is the same in both cases,

$$C_{(m)} = \binom{m}{\frac{m\mp1}{2}} = \frac{m!}{(\frac{m-1}{2})!(\frac{m+1}{2})!}. \tag{2.17}$$

Additionally, and resorting to the example shown in (2.14), we can easily find that each term taken from one ℓ-indexed sub-group is complementary to a term in another $(m-\ell)$-indexed sub-group. Specifically, this property applies to terms with a symmetric distance with respect to the center of the expanded summation. Consequently, according to the complementarity between the central sub-groups in (2.16), it is noteworthy that

$$\Theta\Big(\frac{m+1}{2},\ell'\Big) = -\Theta\Big(\frac{m-1}{2},\ell'\Big) \;\;;\;\; 1 \leq \ell' \leq C_{(m)} \tag{2.18}$$

which allow us to rewrite the braketed (filtered) terms in (2.16) in the form

$$\sum_{\ell'=1}^{C_{(m)}} e^{j[\omega_c t+\alpha_x(t)+\omega_c\Theta(\frac{m+1}{2},\ell')]} + e^{-j[\omega_c t+\alpha_x(t)+\omega_c\Theta(\frac{m+1}{2},\ell')]} \tag{2.19}$$

or, equivalently,

$$2\mathrm{Re}\Big\{\sum_{\ell'=1}^{C_{(m)}} e^{j[\omega_c t+\alpha_x(t)+\omega_c\Theta(\frac{m+1}{2},\ell')]}\Big\}. \tag{2.20}$$

Finally, the bandpass equivalent for the first-zone output of the non-linear model can be expressed as

$$y_1(t) = \mathrm{Re}\Bigg[\sum_{m=1}^{n}\Bigg\{\Bigg[\underbrace{\int_{-\infty}^{\infty}\cdots\int_{-\infty}^{\infty}}_{m-\text{times}} 2h_m(\tau_1,\ldots,\tau_m)\sum_{\ell'=1}^{C_{(m)}} e^{j\omega_c\Theta(\frac{m+1}{2},\ell')}d\tau_m^{\Pi}\Bigg]\Big(\frac{u_x(t)}{2}\Big)^m\Bigg\}e^{j\alpha_x(t)}e^{j\omega_c t}\Bigg] \tag{2.21}$$

which is a functional structure of the form

$$y_1(t) = \mathrm{Re}\Bigg[\Bigg\{\sum_{m=1}^{n} K_m\cdot\Big(\frac{u_x(t)}{2}\Big)^m\Bigg\}e^{j\alpha_x(t)}e^{j\omega_c t}\Bigg] \tag{2.22}$$

where the power terms $\big(\frac{u_x(t)}{2}\big)^m$ account for the AM/AM distortion of the model while the factors

$$K_m = \underbrace{\int_{-\infty}^{\infty}\cdots\int_{-\infty}^{\infty}}_{m-\text{times}} 2h_m(\tau_1,\ldots,\tau_m)\sum_{\ell'=1}^{C_{(m)}} e^{j\omega_c\Theta(\frac{m+1}{2},\ell')}d\tau_m^{\Pi} \tag{2.23}$$

are the complex parameters whose modulus $|K_m|$, along with the power terms of $u_x(t)$, are also involved in the total AM/AM non-linear distortion of the system. In turn, only the phase component is responsible for the AM/PM distortion over the phase $\alpha_x(t)$ of the base-band input signal. Thus, from the non-linear model obtained and expressed in (2.21) to (2.23), we can remark the following:

1. The AM/AM distortion of the model depends only on the variations of the base-band input modulus $u_x(t)$.
2. The structure of AM/PM distortion is determined by the parameter $\Theta(\frac{m+1}{2}, \ell')$.
3. The AM/PM distortion will depend on the carrier frequency f_c and will be affected by significant variations of its value.

The last item suggests an additional analysis of the AM/PM distortion dependence on carrier frequency variations. For convenience, we first rewrite the expression in (2.23) for the terms K_m, including the carrier frequency variation $\Delta\omega_c$. This is accomplished by resorting to the definition of $\Theta(\ell, \ell')$ in terms of the summation $\sum_{i=1}^{m}(\pm)\tau_i$:

$$K_m = 2\sum_{\ell'=1}^{C_{(m)}} \underbrace{\int_{-\infty}^{\infty}\cdots\int_{-\infty}^{\infty}}_{m-\text{times}} h_m(\tau_1,\ldots,\tau_m)\prod_{i=1}^{m} e^{(\pm)j(\omega_c+\Delta\omega_c)\tau_i} d\tau_m^{\Pi}. \tag{2.24}$$

In addition to the narrow-band approximations defined in (2.6), we can make the assumption that $\Delta f_c \cdot \mathcal{T}_i \ll 1$, so that,

$$e^{(\pm)j(\omega_c+\Delta\omega_c)\tau_i} \sim e^{(\pm)j\omega_c\tau_i}(1 + j\Delta\omega_c\mathcal{T}_i). \tag{2.25}$$

According to this, the dependence of the AM/PM distortion will be approximately linear with respect to small variations of the carrier frequency.

In spite of its generality in developing theoretical analysis, the Volterra Series are said to be impractical for most but very few real time applications in which the complexity and cost can be justified. Model designs for practical applications are normally formulated by resorting to the discrete form of the VS [46] [47]. The discrete expressions are suitably simplified by limiting the number of summation terms involved thus providing a P-th order model, sufficiently accurate with regard to the modeling requirements. Basically, as the order of the VSM increases, it will have the same general limitations as the Taylor Series classical approach. Some of these major limitations and impairments of the VSMs are:

- Complex procedures and lengthy measurements are needed to identify the Volterra Kernels.

- The truncation of the series to any P-th order must be justified according to the memory limitation or a priori knowledge of the system.

- Due to its power series character, the VS expansion may converge for only a limited range of input amplitudes.

For these reasons, many researchers have developed higher level models that are readily computable input-to-output characterizations of the nonlinear HPAs. Some of these models even include frequency-dependent extensions that have been developed resorting to experimental data and implicitly assuming the approximation of linear dependence between AM/PM distortion and the carrier frequency variations expressed in (2.25).

2.2 High Level HPA Model for Simulations

There are two different technologies for HPAs commonly used in microwave systems, namely: the traveling-wave tube (TWT) amplifiers and GaAs FET based amplifiers. In particular, the TWT HPAs are known to be more nonlinear than the GaAs FET HPAs and more nonlinear than the Solid State Power Amplifiers (SSPA) in general. Differences are more acute when comparing the AM/PM conversion curves rather than the AM/AM responses [1]. The AM/PM nonlinear conversion of TWTs has been quantified to be nearly 10 times worse than in solid state devices. This severe difference is due to the physics of how the nonlinearity is generated in each device. In the case of TWTs, the AM/PM distortions are caused by mismatches between the microwave phase velocity and the velocity of the electron flux. The ability of electrons to follow the phase variations in the traveling wave slows down as part of their energy is transferred to the wave amplification [48]. A detailed study of the different high level models proposed for representing the nonlinear behaviour of the HPAs falls beyond the scope of this study. Therefore, let us refer to [49] and [44] (chap.2.11) where relevant HPA modeling schemes are analyzed to a larger extent. Among the models available, here we will concentrate in describing the well-known Saleh Model for TWT memoryless HPAs, which is in fact the most commonly used in the literature and thence will be applied later in our PD algorithms evaluation.

2.2.1 The Memoryless Saleh Model for TWT HPAs

It is important to remark at this point, that any linearization algorithm to be described in the forthcoming chapters shall be developed under the perspective of its general applicability and independently from the specific nonlinear model. Nevertheless, for the non-linear distortion of the base-band signal to be applied in the simulations, we select the widely accepted Saleh model [9] for memoryless Traveling Wave Tube Amplifiers (TWTA). Comparatively, Saleh's model introduces more significant AM/PM distortion than most Solid State Power Amplifiers (SSPA) models available [50] [51]. The purpose is hence to provide more stringent conditions to evaluate the linearizing techniques and algorithm performance. Equations (2.26) and (2.27) define this base-band model of HPA as two modulus-dependent transfer functions given by

$$A[u_x] = \frac{\alpha_a u_x}{1 + \beta_a u_x^2} \tag{2.26}$$

$$\Phi[u_x] = \frac{\alpha_\Phi u_x^2}{1 + \beta_\Phi u_x^2} \tag{2.27}$$

where $A[u_x]$ and $\Phi[u_x]$ are the corresponding AM/AM and AM/PM characteristics respectively, both dependent exclusively on u_x, which is the input modulus to the HPA.

In the expressions above, we choose to set the small-signal gain term to $\alpha_a = 2$, while $\beta_a = \beta_\Phi = 1$ and $\alpha_\Phi = \pi/3$, so that the input saturation voltage $A_s = 1/\sqrt{\beta_a}$, and the maximum output amplitude $A_{max} = \max\{A[u_x]\} = \alpha_a A_s/2$, are both normalized to 1. Hence, the phase displacement at the saturation point will be $\Phi_{sat} = \Phi[\, 1/\sqrt{\beta_a}\,] = \pi/6\ [rad] = 30^{\text{o}}$. The corresponding AM/AM and AM/PM curves so scaled are depicted in figure (2.1). These settings are equivalent to the normalization of the input and output signals at the HPA with respect to the corresponding saturation amplitudes, which is useful to represent the amplifier featuring unitary gain at saturation. This normalized characteristics will apply henceforth in our PD implementations and therefore the perfect linear HPA response will be given by the identity function [1].

In the ongoing definitions we use the same base-band signal model defined in (2.3) but now we skip the time dependence for the sake of simplicity. Thus, for the input signal to the HPA,

$$b_x = u_x e^{j\alpha_x}, \tag{2.28}$$

the respective distorted output –assuming memoryless operation– is expressed as

$$b_y = A\,[u_x]\, e^{j(\alpha_x + \Phi[u_x])} \tag{2.29}$$

where the input-output functional relation of the HPA has been defined as a *transfer* function. An alternative expression for the AM/AM distortion in (2.26), convenient for

[1] For experimental input-to-output measures of HPAs, Saleh provided expressions obtained through a minimum MSE fitting procedure for the calculation of the optimum parameters in (2.26) and (2.27).

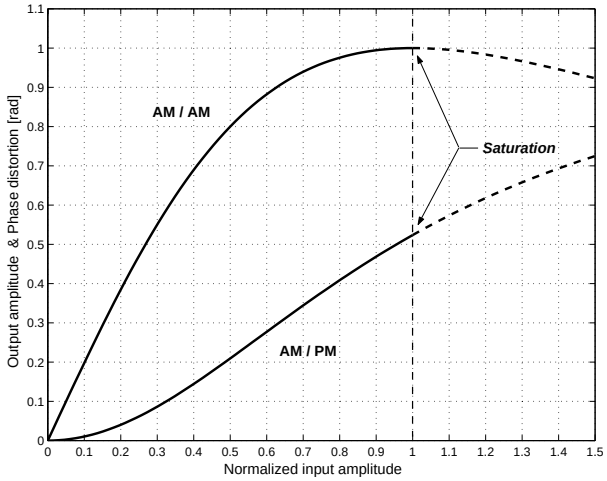

Figure 2.1: AM/AM and AM/PM normalized transfer characteristics of the Saleh model for memoryless TWT HPAs.

the theoretical formulation of the pre-distortion, is obtained by replacing the saturation input amplitude $A_s = 1/\sqrt{\beta_a}$ in the expression (2.26). This gives

$$A[u_x] = \frac{A_s^2 \alpha_a u_x}{A_s^2 + u_x^2} \tag{2.30}$$

whence we can find a theoretical AM/AM inverse[2] transfer function $A^{-1}[\cdot]$ by solving (2.30) for $u_x = A\left[A^{-1}[u_x]\right]$. Some straightforward algebraic steps lead us to directly obtain

$$A^{-1}[u] = \frac{\alpha_a A_s^2}{2u}\left[1 - \sqrt{1 - \left(\frac{2u}{\alpha_a A_s}\right)^2}\right] \tag{2.31}$$

where it is important to note that this inversion will be valid only within the interval $\{\ 0 \leq u \leq \alpha_a A_s/2\ \}$. This defines a restriction for the input range of the theoretical AM/AM PD. However, as will be discussed later, the invertibility of the complex HPA function will not be necessarily restricted to the same limits since they account only for the AM/AM invertibility.

The ideal AM/PM PD characteristic related to the AM/AM theoretical inverse given in (2.31) is much simpler to obtain but not as trivial as taking (2.27) and inverting its sign. This becomes clearer when considering the alternative configurations shown in figure 2.2 where the same PD block, i.e., the same input-output function, is applied as a pre/post-distorter for the linearization of the same HPA. Thus, letting $\Psi[\cdot]$ denote the AM/PM characteristic of the PD block, for the case of a pre-distorter, we have

$$\begin{aligned} b_{pout} &= A^{-1}[u_x] e^{j(\alpha_x + \Psi[u_x])} \\ b_y &= A\left[A^{-1}[u_x]\right] e^{j(\alpha_x + \Psi[u_x] + \Phi[A^{-1}[u_x]])} \end{aligned}$$

[2]In this section the negative exponent denoting inverse functions such as $A^{-1}[\cdot]$ is used only for notation purposes and should not be interpreted as $1/A[\cdot]$.

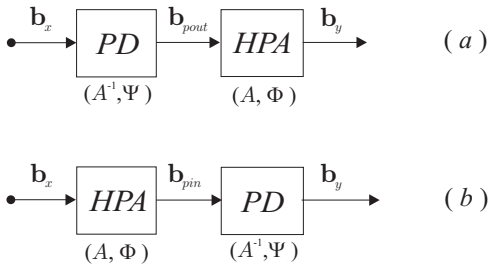

Figure 2.2: Pre-distortion (a) and post-distortion (b) for HPA linearization.

wherein the ideal AM/PM correction requires that

$$\Psi[u_x] = -\Phi[A^{-1}[u_x]]. \tag{2.32}$$

Then, for the post-distorter, we have

$$\begin{aligned} b_{pin} &= A[u_x]e^{j(\alpha_x+\Phi[u_x])} \\ b_y &= A^{-1}\big[A[u_x]\big]e^{j(\alpha_x+\Phi[u_x]+\Psi[A[u_x]])} \end{aligned}$$

where the AM/PM correction now requires that

$$\Psi[A[u_x]] = -\Phi[u_x]. \tag{2.33}$$

Since in both cases we expect that $b_x = b_y$, the conditions expressed in (2.32) and (2.33) are equivalent in the sense that the inverse AM/PM of each given argument must correspond, with opposite sign, to the HPA's straight AM/PM characteristic with the input argument scaled by the inverse AM/AM transfer characteristic $A^{-1}[\cdot]$. Consequently

$$\Psi[u] = -\Phi\left[A^{-1}[u]\right] \tag{2.34}$$

is a general expression for the AM/PM pre/post-distortion function $\Psi[\cdot]$ that compensates for the amplitude-to-phase distortion $\Phi[\cdot]$ introduced by an HPA whose AM/AM nonlinear characteristic $A[\cdot]$ has an exact inverse counterpart $A^{-1}[\cdot]$. Thence, with these conditions fulfiled for the example of figure 2.2, it is true that

$$b_y = A\left[A^{-1}[u_x]\right]e^{j(\alpha_x+\Psi[u_x]+\Phi[A^{-1}[u_x]])} = A^{-1}\big[A[u_x]\big]e^{j(\alpha_x+\Phi[u_x]+\Psi[A[u_x]])} = b_x.$$

Regarding AM/AM PD, we can easily prove that the expression (2.31), found through an ideal pre-distortion hypothesis, can be also applied as a post-distortion function fulfiling the equivalence $A^{-1}\big[A[u_x]\big] = u_x$. A depiction of the ideal theoretic AM/AM and AM/PM inverse characteristics, valid for the normalized Saleh's HPA model in the interval $\{0, 1\}$, is shown in figure 2.3. Note that the shape of the inverse AM/PM does not correspond to $-\Phi[\cdot]$ in accordance with our previous discussion.

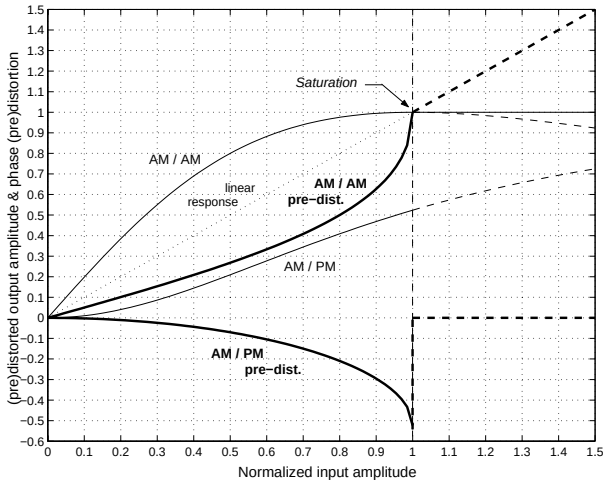

Figure 2.3: AM/AM and AM/PM theoretical pre/post-distortion characteristics for the Saleh model.

The real and imaginary parts of the direct and inverse AM/AM and AM/PM expressions given in (2.26),(2.27), (2.31) and (2.34), are all depicted in figure 2.4 where it is interesting to observe that the real part of the HPA characteristic presents a very similar shape to the AM/AM characteristic. Both curves reach their maximum at relatively close input amplitude points after which they decrease. However, the fact that the real-part "saturation" is located before the HPA saturation does not imply that the HPA characteristic is non-invertible after this point as it is proved by the expression (2.31). This is an interesting aspect deserving our attention and is commented later in section 2.2.2.

In later chapters, it will be shown that for algorithm implementations a good choice is to consider the HPA and the pre/post-distorter as complex gain functions rather than as transfer functions. Let us denote the complex gain function of the HPA as $G_{HPA}[\cdot]$. Thence, the input-output relation at the HPA can be expressed as a multiplicative gain

$$b_{out} = b_{in} G_{HPA}[u_{in}]$$

where the HPA multiplicative gain, which is also dependent on the input modulus $u_{in} = |b_{in}|$, can be decomposed into

$$G_{HPA}[u_{in}] = G_{AM}[u_{in}] G_{PM}[u_{in}] \tag{2.35}$$

$$G_{AM}[u_{in}] = A[u_{in}]/u_{in} = \frac{\alpha_a}{1 + \beta_a u_{in}^2} \tag{2.36}$$

$$G_{PM}[u_{in}] = \cos(\Phi[u_{in}]) + j \sin(\Phi[u_{in}]) \tag{2.37}$$

with $\Phi[\cdot]$ the AM/PM characteristic previously given in (2.27). Note that $G_{PM}[\cdot]$ is a unitary operation defined to only introduce a phase rotation over the input data.

Then, denoting the corresponding theoretical pre-distortion complex gain as $G_{HPA}^{-1}[\cdot]$, with the AM and PM factors named $G_{AM}^{-1}[\cdot]$ and $G_{PM}^{-1}[\cdot]$ respectively, the output of the

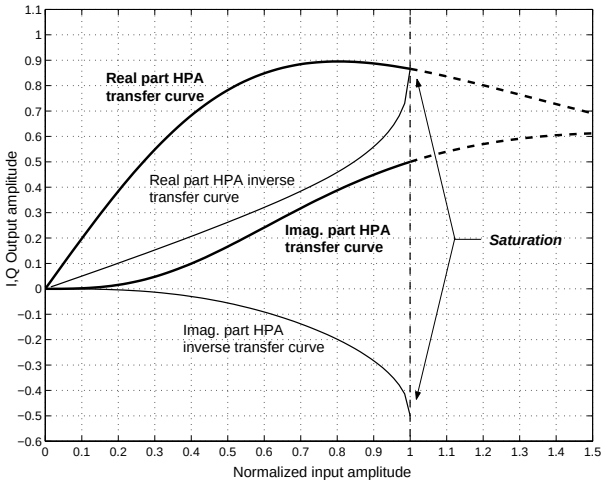

Figure 2.4: Phase and quadrature transfer curves and corresponding pre/post-distortion characteristics for the Saleh model.

PD block in figure 2.2(a) will be given by

$$b_{pout} = b_x G_{HPA}^{-1}[u_x] = b_x G_{AM}^{-1}[u_x] G_{PM}^{-1}[u_{pout}] \tag{2.38}$$

where $u_{pout} = u_x G_{AM}^{-1}[u_x]$. The AM/AM inverse gain is expressed from equation (2.31) as

$$G_{AM}^{-1}[u_x] = \frac{A^{-1}[u_x]}{u_x} = \frac{\alpha_a A_s^2}{2u^2}\left[1 - \sqrt{1 - \left(\frac{2u}{\alpha_a A_s}\right)^2}\right] \tag{2.39}$$

and the AM/PM multiplicative inverse factor, defined by using (2.34), is calculated as

$$G_{PM}^{-1}[u_x] = \cos\big(-\Phi[u_x G_{AM}^{-1}[u_x]]\big) + j\sin\big(\Phi[u_x G_{AM}^{-1}[u_x]]\big). \tag{2.40}$$

Thus, in perfect linearization conditions, the output of the entire linearized chain, in terms of multipliative gains, would be given by

$$\begin{aligned} b_y &= b_x G_{HPA}^{-1}[u_x] G_{HPA}[u_{pout}] && (2.41)\\ &= b_x G_{AM}^{-1}[u_x] G_{PM}^{-1}\big[u_x G_{AM}^{-1}[u_x]\big] G_{AM}\big[u_x G_{AM}^{-1}[u_x]\big] G_{PM}\big[u_x G_{AM}^{-1}[u_x]\big]. && (2.42)\end{aligned}$$

Thence, the ideal AM/AM pre/post-distortion gain should satisfy the following relation:

$$G_{AM}^{-1}[u_x] = \frac{1}{G_{AM}\big[u_x G_{AM}^{-1}[u_x]\big]} \tag{2.43}$$

where we can observe that the estimation of $G_{AM}^{-1}[\cdot]$ is not as straightforward as obtaining the multiplicative inverse of $G_{AM}[\cdot]$ but also involves an inverse transfer identification.

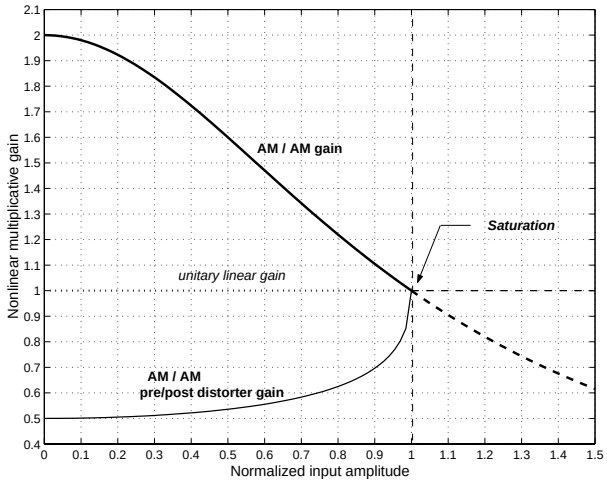

Figure 2.5: AM/AM gain curve for the Saleh model and its corresponding theoretical pre/post-distortion gain.

The AM/PM compensation, in this case, is in turn given by a much simpler relation. In (2.42) the ideal AM/PM PD gain must fulfil

$$G_{PM}^{-1}\big[u_x G_{AM}^{-1}[u_x]\big] = -G_{PM}\big[u_x G_{AM}^{-1}[u_x]\big] \tag{2.44}$$

which is a direct system identification problem, since both functions will always share the same argument. Thence, the required AM/PM PD characteristic will be the same correspondence shown in figure 2.3 whether we estimate the PD using gain or transfer functions. Unlike this, in figure 2.5 we show the ideal AM/AM inverse gain characteristic from (2.39) which completely linearizes the nonlinear model in (2.36), this is, the multiplicative gain equivalent of (2.26).

An interesting alternative way of expressing the nonlinear mapping of an HPA, like the Saleh model, is considering the AM/AM and AM/PM characteristics as part of a parametric function $\mathcal{H}[u_p]$ which is an equivalent nonlinear mapping in a complex cartesian plane as exemplified in figure 2.6. While the independent variable in $A[u_x]$ and $\Phi[u_x]$ was the input modulus to the HPA, in a parametric representation it corresponds to a nonlinear scaling $\mathcal{P}[u_x] = u_p$ such that the new input parameter now corresponds to the total distance measured along the parametric curve from the origin of the complex plane. Thus, the output for a given u_p is a vector on this plane with the amplitude $A[u_x]$ and the phase distortion $\Phi[u_x]$. In this figure we represented in a proportional scale the parametric curves for the HPA model in (2.26) and (2.27) and for its corresponding PD function presented in (2.31) using also (2.34). The AM/AM direct and inverse transfer functions appear as dotted lines and are used to project the vectors over the parametric functions since it is more intuitive than finding, for instance, $\mathcal{P}^{-1}[0.725]$. Thus, in this example, an input vector $\mathbf{x}_{in} = 0.95\angle 0^{\text{o}}$ is applied to the parametric PD resulting in the pre-distorted vector $\mathbf{x}_{pd} = 0.725\angle -\theta^{\text{o}}$ which is in turn applied as the input to the

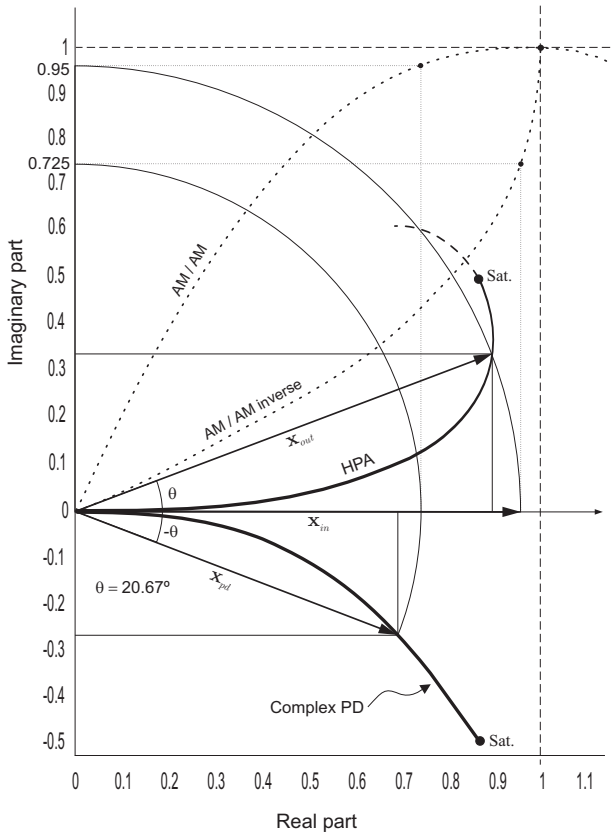

Figure 2.6: Representation of the complex HPA Saleh curve and its pre/post-distortion as parametric I-Q curves.

parametric HPA whose output is finally the vector $\mathbf{x}_{out} = 0.95\angle\theta^{o}$. Clearly, the phases of these last vectors cancel each other thus obtaining a linear unitary transference.

2.2.2 Comments on Invertibility

In the previously presented graphics we have shown the ideal pre-distortion of the Saleh's model HPA up to the saturation point A_s letting the PD response be arbitrarily defined for inputs beyond such level. This is basically due to the limitation found in evaluating the theoretical AM/AM inverse in (2.31). Nevertheless, the 4-parameter expressions of the Saleh model are valid characterizations that fit the measured input-to-output response of real TWTs that, unlike the SSPAs, present a continuous, smooth and non-constant I/O relation in a range that exceeds the AM/AM saturation point as we observed in figure 2.1. In this sense, the nonlinear distortion introduced by an HPA can be divided into two significant categories:

- Distortions originated by the AM/AM and AM/PM nonlinear behaviour of the HPA for input signal values within the 'valid' (under-saturation) input range $[0, A_s]$.

- Distortions due to the saturation imposed by the AM/AM characteristic over the input signal when its amplitude exceeds A_s.

where the former type corresponds to the portion of nonlinear effect that can be effectively counteracted by pre-distorting the input signal through the correct inverse AM/AM and AM/PM curves, while the second type refers to degradations that cannot be compensated by any efficient mean. In practice, we know that the linearization of HPAs achievable with a digital pre-distorter can be defined only within the valid input range that goes from the zero input amplitude to the saturation point. This is logical since digital PDs are adapted using an attenuated and down-converted observation of the real distorted signal at the HPA's output. Thence, a pre-distorter only introduces modifications in the low power base-band signal samples without adding any significant extra power to the input signal to the HPA. This means that ideally the PD will execute a suitable redistribution of the signal energy and therefore, a spectral regrowth effect is expected to take place from the input to the output of the PD after which it is compensated at higher power levels by the HPA distortion.

When the AM/AM transfer (not gain) characteristic of a nonlinear device, given by the complex function $A[|x|]$, presents an absolute maximum A_s, then this maximum determines an upper bound for the output range of the signals transmitted through this device. In such case, we can make a general AM/AM linearization restriction by observing there is no one-to-one pre-mapping $|x| \rightarrow A^{-1}[|x|]$ in the input domain of this nonlinear function, such that, $A\big[A^{-1}[x]\big] > |x_{max}|$, since the AM/AM saturation implies $\{|x|, A^{-1}[|x|]\} \in [|x_{min}|, |x_{max}|]$.

However, this restriction does not apply for the phase component of the signal since its output range is always bounded by $[-\pi, \pi]$ and therefore it is always possible to invert with a PD the nonlinear phase rotation even when $|\Phi[|x|]| > \pi$, as long as the $x \rightarrow \{A[|x|], \Phi[|x|]\}$ mapping is a well defined one-to-one correspondence. This relation is not clearly given in the separated AM/AM and AM/PM modulus-dependent curves which could present two or more images each for the same input amplitude $|x|$ but remain a single-valued I/O correspondence when they are jointly considered as the real and imaginary components of the previously defined parametric function $\mathcal{H}[u_p]$. In the examples of figure 2.7, where u_i denote modulus of the complex input x_{in}, we can distinguish between the linearization and invertibility limits of a complex non-linear characteristic by comparing amplitude-phase transfer pairs with their corresponding parametric representations. In the figure (a) the AM/AM curve reaches saturation after the maximum of the AM/PM. Analytically, the inverse of each separated curve could be well defined only up to the respective maxima A_{sat} and P_{sat}. However, the shaded region that defines the operation zone where an HPA could no longer be linearized under these conditions starts after P_{sat} at u_3. This is because the phase distortion terms for $u_2 \leq |x_{in}| \leq u_3$, which are bi-mapped in the AM/PM curve, correspond to different images in the AM/AM curve and hence the I/O distortion mapping can be identified without ambiguities. Indeed, this example features one-to-one assignation $u_p \rightarrow \mathcal{H}[u_p]$ all along the parametric curve as represented on the right. Therefore, the curve therein

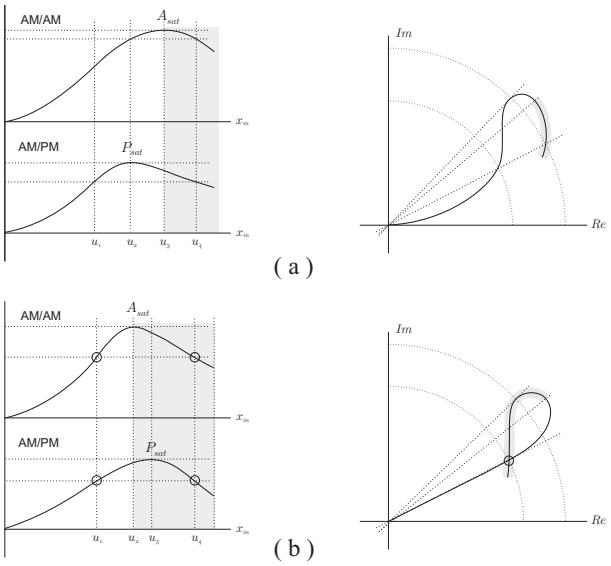

Figure 2.7: Representation of AM/AM and AM/PM characteristics as parametric I-Q curves. In (a) the AM/AM and AM/PM curves feature independent saturation and lead to a unievaluated parametric curve which is therefore invertible. In (b) the circles show the multievaluation of the complex function which means that this characteristic is non-invertible. The shadowed regions show the limit of the invertible region by means of pre-distortion.

shown is completely invertible since it is bijective in its parametric definition. In the second example, in figure 2.7(b), it is shown how the linearizable zone is determined by the AM/AM saturation rather than by the AM/PM maximum. Furthermore, in this example we characterized a critical case where the AM/AM and AM/PM transfer curves coincide in being surjective for the same values x_1 and x_4 in their common domain. As a result of this, the corresponding parametric curve on the right presents a self-intersection point and therefore it corresponds to a non-invertible function.

The algorithms for PD estimation included in this work are capable of compensating for the AM/AM as well as the AM/PM nonlinear distortions. However, their adaptive working principle is based only on information about the input modulus to the PD processor which is conveyed by activation or membership functions. In later chapters it is shown that this is enough information to achieve good linearization performance within the under-saturation region of a nonlinear memoryless HPA. Nevertheless, other applications (probably not involving power amplification) could require the identification of a complex nonlinear function under and over the AM saturation. In such cases, it will be necessary to incorporate phase-mapping information, rather than the unreferenced phase rotation herein used, in order to perform the identification of the inverse parametric function for its subsequent compensation. It is clear that such applications would not be concerned with the same efficiency maximization criteria commonly used in HPA linearization, but they will likely coincide in some error optimization strategies used in the proposed adaptive identification algorithms.

Finally, it is worthy to note that within the range $[0, A_s]$, certain difficulties in linearizing the HPA response can be expected for input values close to the saturation point where the pre-distortion curve variations make the derivaive of $A^{-1}[\cdot]$ tend to infinity. A good approximation to the optimum PD curve in this region would imply a large number of interpolation points to achieve enough resolution to accurately fit the ideal PD. However, increasing the number of interpolating points along the whole curve would constitute a very inefficient solution as it would increase drastically the computational burden. Since this is a relevant parameter for designing an efficient solution for linearization, in the algorithms proposed in this thesis, we will include a technique for the adaptive allocation of a fixed number of interpolation points to be used instead of the uniform augmentation of the resolution along the estimated curves. This technique will be shown through simulations to be an effective tool to adapt the PD in highly nonlinear regions of the gain curve with reduced computational complexity.